

An end-to-end trainable hybrid classical-quantum classifier

Samuel Yen-Chi Chen

E-mail: ychen@bnl.gov
Computational Science Initiative, Brookhaven National Laboratory

Chih-Min Huang

E-mail: b06501134@ntu.edu.tw
Department of Physics, National Taiwan University, Taipei 10617, Taiwan

Chia-Wei Hsing

E-mail: cwhsing0219@gmail.com
Department of Physics, National Taiwan University, Taipei 10617, Taiwan

Ying-Jer Kao

E-mail: yjkao@phys.ntu.edu.tw
Department of Physics, National Taiwan University, Taipei 10617, Taiwan

Abstract. We introduce a hybrid model combining a quantum-inspired tensor network and a variational quantum circuit to perform supervised learning tasks. This architecture allows for the classical and quantum parts of the model to be trained simultaneously, providing an end-to-end training framework. We show that compared to the principal component analysis, a tensor network based on the matrix product state with low bond dimensions performs better as a feature extractor for the input data of the variational quantum circuit in the binary and ternary classification of MNIST and Fashion-MNIST datasets. The architecture is highly adaptable and the classical-quantum boundary can be adjusted according to the availability of the quantum resource by exploiting the correspondence between tensor networks and quantum circuits.

Submitted to: *Machine Learning: Science and Technology*

1. Introduction

Quantum computing (QC) has demonstrated superiority in problems intractable on classical computers [1, 2], such as factorization of large numbers [3] and search in an unstructured database [4]. Recent growth of the quantum volume in noisy intermediate-scale quantum (NISQ) [5] devices has stimulated rapid development in circuit-based quantum algorithms. Due to the noise associated with the quantum gates and lack of quantum error correction on NISQ devices, performing quantum computation with large circuit depth is impossible currently. It is therefore highly desirable to develop quantum algorithms that are resilient to noise with moderate circuit depth. Variational quantum algorithms [6] are a class of algorithms currently under rapid development in many fields. In particular, quantum machine learning (QML) [7, 8, 9] using variational quantum circuits (VQC) shows great potential in surpassing the performance of classical machine learning (ML). One of the major advantages of VQC-based QML compared to its classical counterpart is the drastic reduction in the number of model parameters, potentially mitigating the problem of overfitting common in the classical ML. Moreover, it has been shown that under certain conditions, QML models may learn faster or achieve higher testing accuracies than its classical counterpart [10, 11]. A modern QML architecture typically includes a classical and a quantum part. Famous examples in this hybrid genre include quantum approximate optimization algorithm [12], and quantum circuit learning [13], where the VQC plays an crucial role as the quantum component with the circuit parameters updated via a classical computer. Various architectures and geometries of VQC have been suggested for tasks ranging from binary classification [11, 14, 15, 13] to reinforcement learning [16, 17, 18].

One of the key challenges in the NISQ era is that available quantum hardwares have limited quantum volume and are only capable of executing quantum operations with small circuit-depth. That means that most of the dataset commonly used for classical ML tasks are too large for the NISQ devices. To process the data with input dimension exceeding the number of available qubits, it is necessary to apply dimensional reduction techniques to first compress the input data. For example, in Ref. [19], pre-trained classical deep convolutional neural network is used to compress the high-resolution images into a low dimension representation. However, since the pre-trained model there has a huge number of parameters, it is not clear what is the contribution of the quantum circuit in the whole workload.

On the other hand, a major challenge in building a QML model is how to encode high-dimensional classical data into a quantum circuit efficiently. With the limitation imposed by NISQ in mind, the encoding process should be designed to consume as few gate operations as possible. *Amplitude encoding* is one of the encoding method which can provide significant advantage in terms of the number of qubits required to handle the input data. For an N -dimensional vector, amplitude encoding requires only $\log_2 N$ qubits; however, the quantum circuit depth to prepare such encoded state exceeds the current limits of NISQ devices. Other approaches like single-qubit rotations require only a shallow circuit but it is unclear how to employ such encoding schemes to load high-dimensional data into a quantum circuit. This can be potentially mitigated by preprocessing the input data with classical methods to perform dimension reduction. Principal component analysis (PCA) is a simple dimension reduction method and has been widely used in the QML research; yet it lacks the representation power to retain enough information. More powerful and expressive models such as neural networks

are not commonly utilized due to the requirement of pre-training and the significant number of parameters involved. Therefore, it is necessary to devise a data compression scheme which can be naturally integrated with VQC.

In this paper, we propose a hybrid framework where a matrix product state (MPS) [20, 21], the simplest form of tensor networks (TN) [22], is used as a feature extractor to produce a low dimensional feature vector. This information is subsequently fed into a VQC for classification. Unlike other QML schemes where the classical neural network has to be pre-trained, our framework is trained as a whole. This end-to-end training indicates the quantum-classical boundary can be adjusted based on the available quantum resource. Furthermore, since a MPS can be realized precisely by a quantum circuit [23], it is possible to replace the classical component with a quantum circuit, making the scheme highly adaptable. Our scheme has shown to be superior in the binary classification task for the MNIST dataset [24]. Here, we apply the scheme to more difficult tasks such as the ternary classification of MNIST and the classification tasks of Fashion-MNIST.

The rest of the paper is organized as follows. Section 2 gives a brief introduction to tensor networks and their application in classical ML. Section 3 describes the VQC used in this study. Section 4 introduces the hybrid TN-VQC architecture. The performance of the model is shown in Sec. 5. Finally we conclude in Sec. 6.

2. Tensor Network

Tensor networks are efficient representation of data residing in high-dimensional space. Originally developed in the context of condensed matter physics, TNs have gained attention in the deep learning community, for both theoretical understanding and computational efficiency [25]. They have provided new inspiration for machine learning algorithms and showed encouraging success in both discriminative [26, 27, 28, 29] and generative learning tasks [30]. In addition, the quantum entanglement inherent in the formulation of tensor networks points to a new direction in understanding the mechanism of deep neural networks and may provide a better way to design new network architectures [31, 26].

It is common to use graphical notation to express tensor networks. A tensor is represented as a closed shape, typically a circle, with emanating lines representing tensor indices (Fig. 1). The joined line indicates the corresponding index is contracted, as in the Einstein convention where repeated indices are summed over. The MPS, also known as tensor train, is the simplest TN, and the most widely used tensor networks in physics to study low-dimensional quantum systems, and has recently found application in the field of machine learning [32, 33, 34, 35, 28, 36]. In an MPS, tensors are contracted through the “virtual” indices (α 's in Fig. 1(d)). The dimension of these virtual indices are called bond dimension and is indicated by χ . In the MPS representation of a quantum wave function, the bond dimension indicates the amount of quantum entanglement the MPS can represent in the bond. In the context of ML, this corresponds to the representation power of the MPS.

In the current study, we choose the MPS as our TN for simplicity; there are other examples of TN with distinct entanglement structures such as the tree tensor network (TTN), multi-scale entanglement renormalization ansatz (MERA) and projected entangled pair state (PEPS). The successful application of a specific TN can also give insights into the hidden correlations in the data. The quantumness inherent in the TN gives it great advantage over other architectures in the application of QML. In

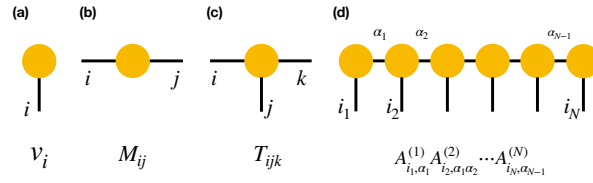


Figure 1. Graphical Notation for Tensors and Tensor Networks. Graphical tensor notation for (a) a vector, (b) a matrix, (c) a rank-3 tensor and (d) a MPS. Here we follow the Einstein convention that repeated indices, represented by internal lines in the diagram, are summed over.

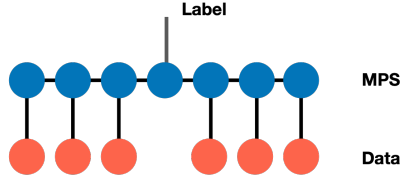


Figure 2. MPS as a feature extractor. Data is encoded into a product state (blue nodes) which is contract with an MPS (yellow node) and a class label is generated.

particular, since each TN can be mapped to a quantum circuit, it means that although in the current scheme, the TN is treated classically, it is possible to replace the whole or part of the TN component by an equivalent quantum circuit when more qubits are available. This gives the current scheme the flexibility to move the quantum-classical boundary based on the available resources.

We will use the MPS as a feature extractor to compress the input data. Following Ref. [33], we approximate a feature extractor by the MPS decomposition as

$$T_{i_1 i_2 \dots i_N}^l = \sum_{\{\alpha\}} A_{i_1, \alpha_1}^{(1)} A_{i_2, \alpha_1 \alpha_2}^{(2)} A_{i_3, \alpha_2 \alpha_3}^{(3)} \dots A_{i_j, \alpha_{j-1} \alpha_{j+1}}^{(j), l} \dots A_{i_N, \alpha_{N-1}}^{(N)}, \quad (1)$$

illustrated in Fig. 2.

3. Variational Quantum Circuit

Variational quantum circuits originates from a quantum algorithm called *variational quantum eigensolver* [37], which is originally used to compute ground states. This family of algorithms have recently drawn significant attention and numerous efforts have been made to extend their applications [6]. VQCs have been successfully applied to function approximation [13, 10], classification [13, 15, 38, 39, 40, 19, 14, 41, 42, 11], generative modeling [43, 44, 45, 46, 47], metric learning [48, 49], deep reinforcement learning [16, 17, 50], sequential learning [10, 51], speech recognition [52] and transfer learning [19]. It has been shown that VQCs are more expressive than conventional neural networks [53, 54, 55, 56] with respect to the number of parameters or the learning speed. It is demonstrated that with similar number of parameters, VQC-based models outperform classical models on testing accuracies [11], and achieve optimal accuracy in function approximation tasks with fewer training epochs than their classical counterparts [10]. Of particular interests for NISQ applications, it has been shown that such circuits are potentially resilient to noises in quantum

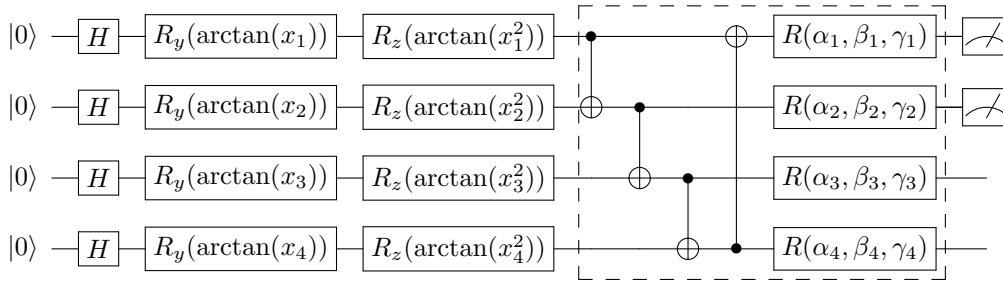


Figure 3. Generic variational quantum circuit architecture. The VQC component used in this work consists of three parts: the encoding part, the variational part with parameters to be learned and the measurement part which will output the Pauli- Z expectation values via multiple run of the quantum circuit. The quantum measurement would be performed on first k qubits where k is the number of classes.

hardware [57, 12, 58], and such robustness has been demonstrated empirically on either noisy simulators or real quantum hardware [49, 16]. This strongly suggests that VQC-based architectures are suitable for building ML applications on NISQ devices.

The VQC used in this work consists of three parts (Fig. 3): The first part is the *encoding* part which consists of Hadamard gate H and single qubit rotation gates $R_y(\arctan(x_i))$ and $R_z(\arctan(x_i^2))$, representing rotations along y -axis and z -axis by the given angle $\arctan(x_i)$ and $\arctan(x_i^2)$, respectively. The Hadamard gate H is used to create unbiased initial state as described Appendix A. Notice the rotation angles $\arctan(x_i)$ and $\arctan(x_i^2)$ are for state preparation and come directly from the input classical data. The data encoding part should be designed with respect to the problem of interest and plays a crucial role in the overall architecture [59]. Potential quantum advantage depends heavily on the encoding scheme together with the hardware limitations incorporated in the design. The second part is the *variational* part which consists of CNOT gates used to entangle quantum states from each qubit and $R(\alpha, \beta, \gamma)$ representing the general single qubit unitary gate with three parameters α_i, β_i and γ_i to be learned. These circuit parameters can be regarded the weights in the classical neural networks. The final part is the *measurement* part which will output the Pauli- Z expectation values via multiple run of the quantum circuit. The retrieved values (logits) will go through classical processing such as softmax to generate the *probability* of each possible class. The quantum measurement would be performed on first k qubits where k is the number of classes.

4. Hybrid TN-VQC Architecture

Figure 4 shows the architecture of the hybrid TN-VQC model. The input image of $N = 28 \times 28 = 784$ pixels from MNIST or Fashion-MNIST is flattened into a 784-dimensional vector $\mathbf{x} = (x_1, x_2, \dots, x_N)$, and each component is normalized such that $x_i \in [0, 1]$. The vector is mapped to a product state using the feature map [33]

$$\mathbf{x} \rightarrow |\Phi(\mathbf{x})\rangle = \begin{bmatrix} x_1 \\ 1 - x_1 \end{bmatrix} \otimes \begin{bmatrix} x_2 \\ 1 - x_2 \end{bmatrix} \otimes \dots \otimes \begin{bmatrix} x_N \\ 1 - x_N \end{bmatrix}, \quad (2)$$

and further process by the MPS to generate a compressed representation. The feature vector is then encoded into the quantum circuit using the variational encoding

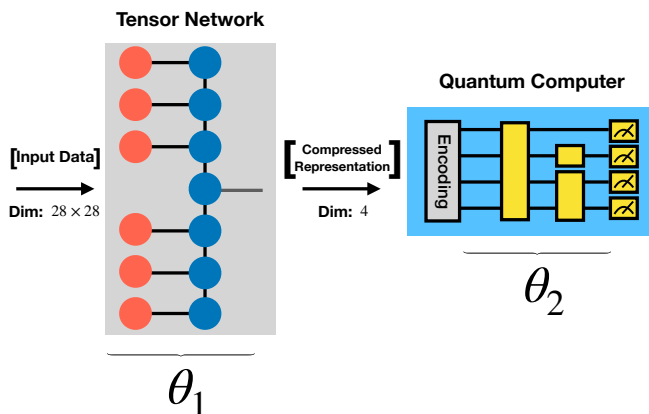


Figure 4. Hybrid TN-VQC Architecture. The tunable parameters labeled with θ_1 and θ_2 are the parameters for the MPS and VQC respectively. See text for details.

(See Appendix A). At the end of the VQC, the quantum measurement would be performed to generate the logits for classification. Both the TN and VQC have tunable parameters, labeled as θ_1 and θ_2 respectively in Fig. 4, which are optimized via gradient descent methods. Gradients of the quantum circuit parameters are calculated using the *parameter-shift* method (See Appendix B), which avoids the use of finite difference calculation. This method is similar to the computation of gradients in neural networks; therefore, the end-to-end training of this TN-VQC model follows the standard backpropagation method as in the training of deep neural networks, and no pre-trained classical model is needed.

Since the classical and quantum parts of the model can be trained simultaneously, it allows for more flexibility in terms of implementation on the quantum hardware. When more qubits are available, one simply increases the dimension of the feature vector out of the MPS to match the input of the VQC and retrain the model. On the other hand, the modular architecture also has the advantage that the classical and quantum parts can be reused independently. For example, it is possible to perform transfer learning by freezing the parameters in the MPS/VQC and training the other part to tackle different types of problems.

5. Experiments and Results

We study the capabilities of the hybrid TN-VQC architecture by performing classification tasks on the standard benchmark dataset MNIST [60] and Fashion-MNIST [61]. Results for the binary classification of MNIST have been presented in Ref. [24]. Here, we perform ternary classification for MNIST and both binary and ternary classifications for Fashion-MNIST. As a baseline, we perform the same tasks on a hybrid PCA-VQC model, where the PCA part serves as the simple feature extractor and the VQC as the classifier. As a comparison, we also present results using the MPS as a classifier to demonstrate the role of VQC in the workload. The computational tools we use for the simulation of variational quantum circuits and tensor networks are PyTorch [62], PennyLane [63] and Qulacs [64]. Details of the simulations such as

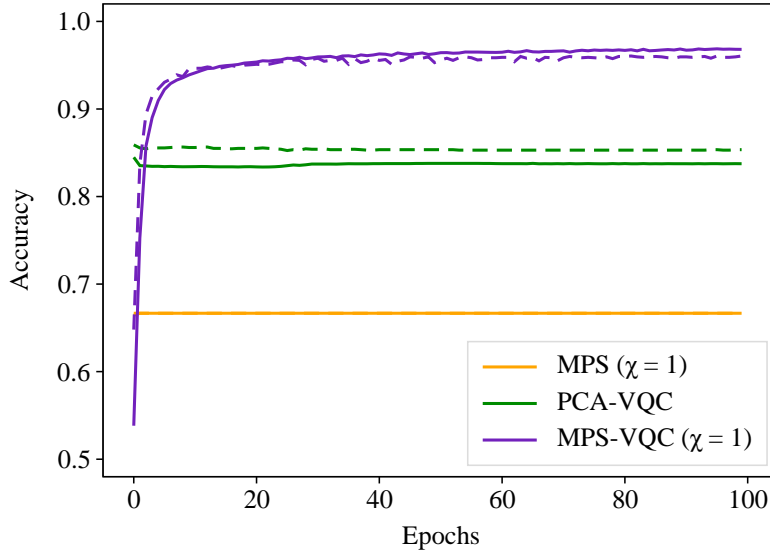


Figure 5. Binary classification of class 5 and 7. Results of the binary classification of Fashion-MNIST (class 5 vs 7). Solid line: training accuracy. Dashed line: test accuracy

the hyperparameters and optimizers for each experiment are summarized in Appendix C.

5.1. Binary Classification

We perform binary classification of the Fashion-MNIST dataset (class 5 vs 7), which is a more difficult task than the binary classification of MNIST performed in Ref. [24]. The results from different models are shown in Fig. 5. For the MPS classifier and the MPS-VQC model, bond dimension $\chi = 1$ is demonstrated. It is evident from both the training and test accuracy that such a bond dimension, while insufficient for the MPS classifier to yield good results, is enough for the MPS-VQC hybrid model to learn properly and reach a test accuracy around 96%. As the number of parameters of the VQC part is far fewer than that of the MPS, this suggests that our VQC possess greater power in classification and dominates the workload. It is also clear that MPS, compared to PCA, serves as a better feature extractor for a VQC discriminator. For a more difficult dataset, we expect that a higher bond dimension will be needed.

5.2. Ternary Classification

In the ternary classification, we consider both the MNIST (class 0, 3, 6) and Fashion-MNIST (class 5, 7, 9) datasets. The results for the MPS-VQC model and the baseline model PCA-VQC are shown in Figure 6. Since ternary classification is a more difficult task, a larger bond dimension is required for the MPS part. In terms of performance, all show that the MPS is superior to the PCA as a feature extractor. With $\chi = 2$, MPS-VQC is able to reach a test accuracy over 98% in MNIST and 92% in Fashion-MNIST. Furthermore, the representation power of an MPS feature extractor is tunable

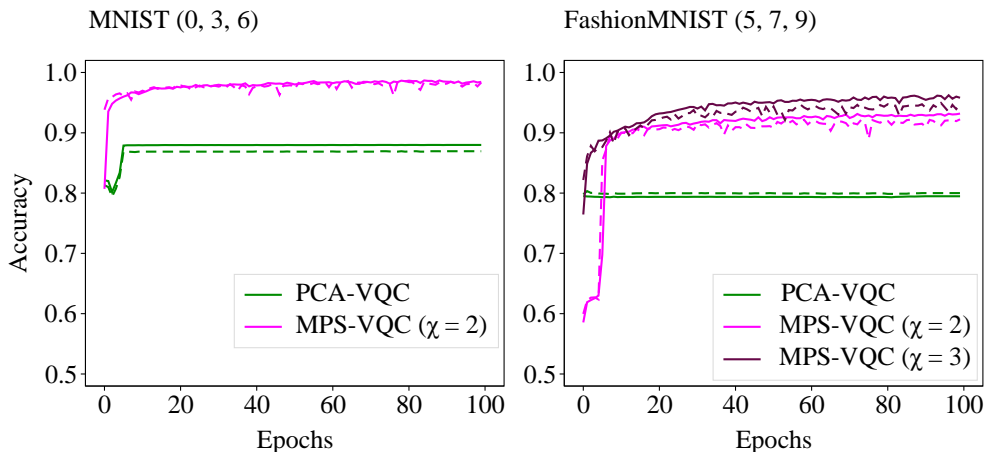


Figure 6. Ternary classification of MNIST and Fashion-MNIST. Results of the ternary classification of MNIST (class 0, 3, 6) and Fashion-MNIST (class 5, 7, 9). Solid line: training accuracy. Dashed line: test accuracy.

via χ , which is an advantage absent in PCA. In the case of Fashion-MNIST, we observe a 2% increase in test accuracy as the bond dimension increases, indicating a better data compression capability due to the increased representation power of the MPS. It is clear that for more complex classification problems, the performance of PCA-VQC should further deteriorate while that of MPS-VQC can be increased by increasing χ .

6. Conclusion

In this work, we present a hybrid quantum-classical classifier by integrating a quantum-inspired tensor network and a variational quantum circuit. Such a hybrid TN-VQC architecture enables researchers to build QML applications capable of dealing with larger dimensional inputs and potentially to implement these QML models on NISQ devices with limited number of qubits and shallow circuit depth. We further demonstrate the superiority of this framework by comparing it with the baseline study of a PCA-VQC model on ternary classification task on the MNIST and Fashion-MNIST dataset as well as a binary classification task of the Fashion-MNIST dataset. One clear advantage is that the representation power of the trainable MPS feature extractor is tunable with the bond dimension of the tensors. Our results point to future application of the hybrid TN-VQC model in different quantum machine learning scenarios and potentially implementation on NISQ devices. Extension of this architecture to more complicated datasets such as CIFAR-10 should further test the robustness and capability of the model. We note this requires more computing resources and better optimized simulators. The proposed hybrid model can be integrated with various kinds of TNs or VQCs, given the suitable encoding methods. For example, one can replace the MPS by other TNs with other entanglement structure such as TTN, MERA and PEPS, whose potential in the supervised learning context has been demonstrated [27, 29, 65]. They may serve also good feature extractors for datasets that contain special structure and correlations. Another way to build a more sophisticated feature extractor is to stack multiple TN layers. It has been shown

that stacking more layers in classical deep neural networks can increase the model performance [66, 67]. Attempts to build a deep convolutional tensor network [68] does not show the same improvement generally observed in classical deep neural network. We can also replace the simple VQC in our architecture with novel VQC architectures such as the quantum convolutional neural networks [11, 69, 70, 71, 72, 73, 74, 75]. How to apply these ideas to improve the performance of the current model is worth further investigation.

This work is supported (in part) by the U.S. DOE under grant No. DE-SC-0012704 and the BNL LDRD No.20-024 and Ministry of Science and Technology (MOST) of Taiwan under grants No. 108-2112-M-002-020-MY3 and No. 107-2112-M-002-016-MY3.

Appendix A. Encoding into Quantum States

In our hybrid framework, the outputs from the classical parts need to be encoded such that they can be used by the quantum circuit. A general N -qubit quantum state can be represented as:

$$|\psi\rangle = \sum_{(q_1, q_2, \dots, q_N) \in \{0,1\}^N} c_{q_1, \dots, q_N} |q_1\rangle \otimes |q_2\rangle \otimes |q_3\rangle \otimes \dots \otimes |q_N\rangle, \quad (\text{A.1})$$

where c_{q_1, \dots, q_N} are complex numbers. They are *amplitudes* of each quantum state and $q_i \in \{0, 1\}$. The square of the amplitude c_{q_1, \dots, q_N} represents the *probability* of measurement results in $|q_1\rangle \otimes |q_2\rangle \otimes |q_3\rangle \otimes \dots \otimes |q_N\rangle$, and the total probability should sum to 1, i.e.,

$$\sum_{(q_1, q_2, \dots, q_N) \in \{0,1\}^N} |c_{q_1, \dots, q_N}|^2 = 1. \quad (\text{A.2})$$

In this work, we choose the *variational encoding* method to encode our classical data into the quantum states. The initial quantum state $|0\rangle \otimes \dots \otimes |0\rangle$ first undergoes the $H \otimes \dots \otimes H$ operation to create the unbiased state $|+\rangle \otimes \dots \otimes |+\rangle$, where H is the Hadamard gate. Consider a n -qubit system, the corresponding unbiased initial state is,

$$\begin{aligned} (H|0\rangle)^{\otimes n} &= \underbrace{H|0\rangle \otimes \dots \otimes H|0\rangle}_n \\ &= \underbrace{|+\rangle \otimes \dots \otimes |+\rangle}_n \\ &= \underbrace{\left[\frac{1}{\sqrt{2}} (|0\rangle + |1\rangle) \right] \otimes \dots \otimes \left[\frac{1}{\sqrt{2}} (|0\rangle + |1\rangle) \right]}_n \\ &= \left[\frac{1}{\sqrt{2}} (|0\rangle + |1\rangle) \right]^{\otimes n} \\ &= \frac{1}{\sqrt{2^n}} (|0\rangle + |1\rangle)^{\otimes n} \\ &= \frac{1}{\sqrt{2^n}} (|0\rangle \otimes \dots \otimes |0\rangle + \dots + |1\rangle \otimes \dots \otimes |1\rangle) \end{aligned}$$

$$= \frac{1}{\sqrt{2^n}} \sum_{k=0}^{2^n-1} |k\rangle, \quad (\text{A.3})$$

This initial quantum state will first go through the encoding part which consists of R_y and R_z rotations. These rotation operations are parameterized by the input vector $\vec{x} = (x_1, x_2, \dots, x_n)$. On the i -th qubit with $i = 1 \dots n$, R_y rotates the state by an angle of $\arctan(x_i)$ and R_z by $\arctan(x_i^2)$. The encoded state is then processed with the variational quantum circuits with optimizable parameters, as shown in the dashed-box in Fig. 3.

Appendix B. Calculation of Gradients of Quantum Functions

Here the models are trained via gradient-descent methods widely used in training the deep neural network. To calculate the gradients with respect to the parameters of quantum circuits, we employ the *parameter-shift* method [76, 63, 13]. Given the knowledge of computing the expectation values of an observable \hat{P} on quantum function,

$$f(\mathbf{x}; \theta_i) = \langle 0 | U_0^\dagger(\mathbf{x}) U_i^\dagger(\theta_i) \hat{P} U_i(\theta_i) U_0(\mathbf{x}) | 0 \rangle = \langle x | U_i^\dagger(\theta_i) \hat{P} U_i(\theta_i) | x \rangle, \quad (\text{B.1})$$

where \mathbf{x} is the classical input vector (e.g. the output values from the PCA or MPS parts), $U_0(x)$ is the quantum encoding routine to prepare the classical value x into a quantum state, i is the circuit parameter index for which the gradient is to be evaluated, and $U_i(\theta_i)$ represents the single-qubit rotation generated by the Pauli operators X, Y, Z . It can be shown [13] that the gradient of this quantum function f with respect to the parameter θ_i is

$$\nabla_{\theta_i} f(x; \theta_i) = \frac{1}{2} \left[f\left(x; \theta_i + \frac{\pi}{2}\right) - f\left(x; \theta_i - \frac{\pi}{2}\right) \right]. \quad (\text{B.2})$$

Appendix C. Computational details

Here we summarize the optimizer and hyperparameters in our experiments.

- MPS classifier: In experiments where MPS alone is used as a classifier, the optimizer is Adam [77] with a learning rate of 0.001 and batch size of 100.
- PCA-VQC model: In our baseline model, PCA is used to reduce the input dimension of $28 \times 28 = 784$ into a four-dimensional vector and is implemented with the Python package scikit-learn [78]. For the VQC classifier, the optimizer is RMSProp [79] with the hyperparameters: learning rate = 0.01, $\alpha = 0.99$ and $\epsilon = 10^{-8}$.
- MPS-VQC hybrid model: In the hybrid TN-VQC architecture, the optimizer is Adam [77] with a learning rate of 0.0001 and batch size of 50. The VQC consists of four variational blocks (dashed-line box in Figure 3). The number of quantum circuit parameters is $4 \times 4 \times 3 = 48$ in this setting. The quantum measurement at the final part of a VQC depends on the number of classes to be classified. For binary classification tasks, the first two qubits are measured, whereas for ternary classification, we perform quantum measurement on the first three qubits.

In all cases, we use cross entropy loss as our loss function.

References

- [1] Harrow A W and Montanaro A 2017 *Nature* **549** 203–209
- [2] Nielsen M A and Chuang I 2002 Quantum computation and quantum information
- [3] Shor P W 1999 *SIAM review* **41** 303–332
- [4] Grover L K 1997 *Physical review letters* **79** 325
- [5] Preskill J 2018 *Quantum* **2** 79
- [6] Cerezo M, Arrasmith A, Babbush R, Benjamin S C, Endo S, Fujii K, McClean J R, Mitarai K, Yuan X, Cincio L *et al.* 2020 *arXiv preprint arXiv:2012.09265*
- [7] Schuld M and Petruccione F 2018 *Supervised learning with quantum computers* vol 17 (Springer)
- [8] Biamonte J, Wittek P, Pancotti N, Rebentrost P, Wiebe N and Lloyd S 2017 *Nature* **549** 195–202
- [9] Dunjko V and Briegel H J 2018 *Reports on Progress in Physics* **81** 074001
- [10] Chen S Y C, Yoo S and Fang Y L L 2020 *arXiv preprint arXiv:2009.01783*
- [11] Chen S Y C, Wei T C, Zhang C, Yu H and Yoo S 2020 *arXiv preprint arXiv:2012.12177*
- [12] Farhi E, Goldstone J and Gutmann S 2014 *arXiv preprint arXiv:1411.4028*
- [13] Mitarai K, Negoro M, Kitagawa M and Fujii K 2018 *Physical Review A* **98** 032309
- [14] Abohashima Z, Elhosen M, Houssein E H and Mohamed W M 2020 *arXiv preprint arXiv:2006.12270*
- [15] Schuld M, Bocharov A, Svore K M and Wiebe N 2020 *Physical Review A* **101** 032308
- [16] Chen S Y C, Yang C H H, Qi J, Chen P Y, Ma X and Goan H S 2020 *IEEE Access* **8** 141007–141024
- [17] Lockwood O and Si M 2020 Reinforcement learning with quantum variational circuit *Proceedings of the AAAI Conference on Artificial Intelligence and Interactive Digital Entertainment* vol 16 pp 245–251
- [18] Wu S, Jin S, Wen D and Wang X 2020 *arXiv preprint arXiv:2012.10711*
- [19] Mari A, Bromley T R, Izaac J, Schuld M and Killoran N 2019 *arXiv preprint arXiv:1912.08278*
- [20] Östlund S and Rommer S 1995 *Phys. Rev. Lett.* **75**(19) 3537–3540 URL <https://link.aps.org/doi/10.1103/PhysRevLett.75.3537>
- [21] Schollwöck U 2011 *Annals of physics* **326** 96–192
- [22] Orús R 2014 *Annals of Physics* **349** 117 – 158 ISSN 0003-4916 URL <http://www.sciencedirect.com/science/article/pii/S0003491614001596>
- [23] Huggins W, Patil P, Mitchell B, Whaley K B and Stoudenmire E M 2019 *Quantum Science and Technology* **4** 024001 (*Preprint* 1803.11537)
- [24] Chen S Y C, Huang C M, Hsing C W and Kao Y J 2020 Hybrid quantum-classical classifier based on tensor network and variational quantum circuit (*Preprint* 2011.14651)
- [25] Orús R 2019 *Nature Reviews Physics* **1** 538–550 URL <https://doi.org/10.1038/s42254-019-0086-7>
- [26] Levine Y, Yakira D, Cohen N and Shashua A 2018 Deep learning and quantum entanglement: Fundamental connections with implications to network design *International Conference on Learning Representations*
- [27] Stoudenmire E M 2018 *Quantum Science and Technology* **3** 034003
- [28] Liu D, Ran S J, Wittek P, Peng C, García R B, Su G and Lewenstein M 2019 *New Journal of Physics* **21** 073059 (*Preprint* 1710.04833)
- [29] Reyes J and Stoudenmire M 2020 *arXiv (Preprint* 2001.08286)
- [30] Han Z Y, Wang J, Fan H, Wang L and Zhang P 2018 *Phys. Rev. X* **8**(3) 031012 URL <https://link.aps.org/doi/10.1103/PhysRevX.8.031012>
- [31] Levine Y, Sharir O, Cohen N and Shashua A 2019 *Physical Review Letters* **122** 065301 ISSN 0031-9007 (*Preprint* 1803.09780)
- [32] Cohen N, Sharir O and Shashua A 2016 On the expressive power of deep learning: A tensor analysis *Conference on learning theory* pp 698–728
- [33] Stoudenmire E M and Schwab D J 2016 *Advances in Neural Information Processing Systems* **29** 4799 (*Preprint* 1605.05775) URL <http://arxiv.org/abs/1605.05775>
- [34] Bengua J A, Phien H N and Tuan H D 2015 Optimal feature extraction and classification of tensors via matrix product state decomposition *2015 IEEE International Congress on Big Data* pp 669–672
- [35] Novikov A, Podoprikin D, Osokin A and Vetrov D 2015 Tensorizing neural networks (*Preprint* 1509.06569)
- [36] Efthymiou S, Hidary J and Leichenauer S 2019 Tensornetwork for machine learning (*Preprint* 1906.06329)
- [37] Peruzzo A, McClean J, Shadbolt P, Yung M H, Zhou X Q, Love P J, Aspuru-Guzik A and O’Brien J L 2014 *Nature communications* **5** 4213

- [38] Havlíček V, Córcoles A D, Temme K, Harrow A W, Kandala A, Chow J M and Gambetta J M 2019 *Nature* **567** 209–212
- [39] Farhi E and Neven H 2018 *arXiv preprint arXiv:1802.06002*
- [40] Benedetti M, Lloyd E, Sack S and Fiorentini M 2019 *Quantum Science and Technology* **4** 043001
- [41] Easom-McCaldin P, Bouridane A, Belatreche A and Jiang R 2020 *arXiv preprint arXiv:2008.12616*
- [42] Sarma A, Chatterjee R, Gili K and Yu T 2019 *arXiv preprint arXiv:1909.04226*
- [43] Dallaire-Demers P L and Killoran N 2018 *Physical Review A* **98** 012324
- [44] Stein S A, Baheri B, Tischio R M, Mao Y, Guan Q, Li A, Fang B and Xu S 2020 *arXiv preprint arXiv:2010.09036*
- [45] Zoufal C, Lucchi A and Woerner S 2019 *npj Quantum Information* **5** 1–9
- [46] Situ H, He Z, Li L and Zheng S 2018 *arXiv preprint arXiv:1807.01235*
- [47] Nakaji K and Yamamoto N 2020 *arXiv preprint arXiv:2010.13727*
- [48] Lloyd S, Schuld M, Ijaz A, Izaac J and Killoran N 2020 *arXiv preprint arXiv:2001.03622*
- [49] Nghiem N A, Chen S Y C and Wei T C 2020 *arXiv preprint arXiv:2010.13186*
- [50] Jerbi S, Trenkwalder L M, Nautrup H P, Briegel H J and Dunjko V 2019 *arXiv preprint arXiv:1910.12760*
- [51] Bausch J 2020 *arXiv preprint arXiv:2006.14619*
- [52] Yang C H H, Qi J, Chen S Y C, Chen P Y, Siniscalchi S M, Ma X and Lee C H 2020 *arXiv preprint arXiv:2010.13309*
- [53] Sim S, Johnson P D and Aspuru-Guzik A 2019 *Advanced Quantum Technologies* **2** 1900070
- [54] Lanting T, Przybysz A J, Smirnov A Y, Spedalieri F M, Amin M H, Berkley A J, Harris R, Altomare F, Boixo S, Bunyk P *et al.* 2014 *Physical Review X* **4** 021041
- [55] Du Y, Hsieh M H, Liu T and Tao D 2020 *Phys. Rev. Research* **2**(3) 033125 URL <https://link.aps.org/doi/10.1103/PhysRevResearch.2.033125>
- [56] Abbas A, Sutter D, Zoufal C, Lucchi A, Figalli A and Woerner S 2020 *arXiv preprint arXiv:2011.00027*
- [57] Kandala A, Mezzacapo A, Temme K, Takita M, Brink M, Chow J M and Gambetta J M 2017 *Nature* **549** 242–246
- [58] McClean J R, Romero J, Babbush R and Aspuru-Guzik A 2016 *New Journal of Physics* **18** 023023
- [59] Schuld M and Petruccione F 2018 Information encoding *Supervised Learning with Quantum Computers* (Cham: Springer International Publishing) pp 139–171 ISBN 978-3-319-96424-9 URL https://doi.org/10.1007/978-3-319-96424-9_5
- [60] LeCun Y <http://yann.lecun.com/exdb/mnist/>
- [61] Xiao H, Rasul K and Vollgraf R 2017 Fashion-mnist: a novel image dataset for benchmarking machine learning algorithms (*Preprint* 1708.07747)
- [62] Paszke A, Gross S, Massa F, Lerer A, Bradbury J, Chanan G, Killeen T, Lin Z, Gimelshein N, Antiga L *et al.* 2019 Pytorch: An imperative style, high-performance deep learning library *Advances in neural information processing systems* pp 8026–8037
- [63] Bergholm V, Izaac J, Schuld M, Gogolin C, Blank C, McKiernan K and Killoran N 2018 *arXiv preprint arXiv:1811.04968*
- [64] Suzuki Y, Kawase Y, Masumura Y, Hiraga Y, Nakadai M, Chen J, Nakanishi K M, Mitarai K, Imai R, Tamiya S *et al.* 2020 *arXiv preprint arXiv:2011.13524*
- [65] Glasser I, Pancotti N and Cirac J I 2019 From probabilistic graphical models to generalized tensor networks for supervised learning (*Preprint* 1806.05964)
- [66] Szegedy C, Liu W, Jia Y, Sermanet P, Reed S, Anguelov D, Erhan D, Vanhoucke V and Rabinovich A 2015 Going deeper with convolutions *Proceedings of the IEEE conference on computer vision and pattern recognition* pp 1–9
- [67] Simonyan K and Zisserman A 2015 Very deep convolutional networks for large-scale image recognition *International Conference on Learning Representations*
- [68] Blagoveschensky P and Phan A H 2020 *arXiv preprint arXiv:2005.14506*
- [69] Cong I, Choi S and Lukin M D 2019 *Nature Physics* **15** 1273–1278
- [70] Li Y, Zhou R G, Xu R, Luo J and Hu W 2020 *Quantum Science and Technology* **5** 044003
- [71] Oh S, Choi J and Kim J 2020 *arXiv preprint arXiv:2009.09423*
- [72] Kerenidis I, Landman J and Prakash A 2019 *arXiv preprint arXiv:1911.01117*
- [73] Henderson M, Shakya S, Pradhan S and Cook T 2020 *Quantum Machine Intelligence* **2** 1–9
- [74] Liu J, Lim K H, Wood K L, Huang W, Guo C and Huang H L 2019 *arXiv preprint arXiv:1911.02998*
- [75] Pesah A, Cerezo M, Wang S, Volkoff T, Sornborger A T and Coles P J 2020 *arXiv preprint arXiv:2011.02966*

- [76] Schuld M, Bergholm V, Gogolin C, Izaac J and Killoran N 2019 *Physical Review A* **99** 032331
- [77] Kingma D P and Ba J 2014 *arXiv preprint arXiv:1412.6980*
- [78] Pedregosa F, Varoquaux G, Gramfort A, Michel V, Thirion B, Grisel O, Blondel M, Prettenhofer P, Weiss R, Dubourg V, Vanderplas J, Passos A, Cournapeau D, Brucher M, Perrot M and Duchesnay E 2011 *Journal of Machine Learning Research* **12** 2825–2830
- [79] Tieleman T and Hinton G 2012 Lecture 6.5—RmsProp: Divide the gradient by a running average of its recent magnitude COURSERA: Neural Networks for Machine Learning